THE JOURNAL OF BIOLOGICAL CHEMISTRY VOL. 287, NO. 24, pp. 19856–19869, June 8, 2012

Ca^{2+}/Calmodulin-dependent Protein Kinase II (CaMKII) Regulates Cardiac Sodium Channel $Na_V1.5$ Gating by Multiple Phosphorylation Sites*[S]

Received for publication, November 10, 2011, and in revised form, April 13, 2012 Published, JBC Papers in Press, April 18, 2012, DOI 10.1074/jbc.M111.322537

Nicole M. Ashpole[‡1], Anthony W. Herren[§1], Kenneth S. Ginsburg[§], Joseph D. Brogan[‡], Derrick E. Johnson[‡], Theodore R. Cummins[‡], Donald M. Bers[§2], and Andy Hudmon[‡3]

From the [‡]Indiana University School of Medicine, Indianapolis, Indiana 46202 and the [§]University of California Davis School of Medicine, Davis, California 95616

Background: CaMKII is up-regulated in heart failure and modulates Na^+ current (I_{Na}), yet the mechanism is unclear.
Result: CaMKII phosphorylates several sites in the first intracellular loop of $Na_V1.5$, thereby altering I_{Na} gating properties.
Conclusion: This multisite phosphorylation may contribute to acquired arrhythmogenesis.
Significance: Identification of these regulatory sites is critical for potential therapeutic targeting of CaMKII and $Na_V1.5$ in failing hearts.

The cardiac Na^+ channel $Na_V1.5$ current (I_{Na}) is critical to cardiac excitability, and altered I_{Na} gating has been implicated in genetic and acquired arrhythmias. Ca^{2+}/calmodulin-dependent protein kinase II (CaMKII) is up-regulated in heart failure and has been shown to cause I_{Na} gating changes that mimic those induced by a point mutation in humans that is associated with combined long QT and Brugada syndromes. We sought to identify the site(s) on $Na_V1.5$ that mediate(s) the CaMKII-induced alterations in I_{Na} gating. We analyzed both CaMKII binding and CaMKII-dependent phosphorylation of the intracellularly accessible regions of $Na_V1.5$ using a series of GST fusion constructs, immobilized peptide arrays, and soluble peptides. A stable interaction between δ_C-CaMKII and the intracellular loop between domains 1 and 2 of $Na_V1.5$ was observed. This region was also phosphorylated by δ_C-CaMKII, specifically at the Ser-516 and Thr-594 sites. Wild-type (WT) and phosphomutant $hNa_V1.5$ were co-expressed with GFP-δ_C-CaMKII in HEK293 cells, and I_{Na} was recorded. As observed in myocytes, CaMKII shifted WT I_{Na} availability to a more negative membrane potential and enhanced accumulation of I_{Na} into an intermediate inactivated state, but these effects were abolished by mutating either of these sites to non-phosphorylatable Ala residues. Mutation of these sites to phosphomimetic Glu residues negatively shifted I_{Na} availability without the need for CaMKII. CaMKII-dependent phosphorylation of $Na_V1.5$ at multiple sites (including Thr-594 and Ser-516) appears to be required to evoke loss-of-function changes in gating that could contribute to acquired Brugada syndrome-like effects in heart failure.

Inward Na^+ current (I_{Na})[4] in the heart is produced primarily by the $Na_V1.5$ channel. I_{Na} is responsible for the rapid upstroke of the cardiac myocyte action potential and for rapid propagation of depolarization throughout the heart. I_{Na} normally activates and inactivates very rapidly, but genetic or acquired alterations in cardiac sodium channel gating can lead to long QT syndrome (where I_{Na} fails to completely inactivate) and Brugada syndrome (where I_{Na} availability is reduced), which can predispose patients to ventricular arrhythmias (1). Moreover, one human $Na_V1.5$ mutation (1795InsD) is associated with both long QT syndrome at low heart rates and Brugada syndrome at high heart rates (2). These genetic channelopathies, although relatively rare, have been extremely important in understanding the arrhythmogenic basis of channel gating alterations. Genetically normal channels may exhibit altered channel gating due to acquired post-translational modifications that may accompany common diseases, such as ischemic heart disease and heart failure (3).

Ca^{2+}/calmodulin (CaM)-dependent protein kinase II (CaMKII) expression and activity levels are increased in both animal models of heart failure and in failing human hearts (4–7). CaMKII also co-immunoprecipitates with and phosphorylates $Na_V1.5$ in cardiomyocytes (8). Overexpression of δ_C-CaMKII, the predominant cardiac myocyte isoform, either acutely in rabbit myocytes or transgenically in mouse myocytes, produces complex effects on I_{Na} gating (8). Notably, these effects phenocopy the human $Na_V1.5$ mutation (1795InsD), which causes combined long QT syndrome and Brugada syndrome (2). These include a hyperpolarizing shift in voltage dependence of availability, enhanced intermediate inactivation, and slowed recovery from intermediate inactivation, all of

* This work was supported, in whole or in part, by National Institutes of Health Grants NS053422 (to T. R. C.), P01-HL080101 (to D. M. B.), and R37HL30077 (to D. M. B.). This work was also supported by American Heart Association National Scientist Development Grant 0930064N (to A. H.) and a grant from the Ralph W. and Grace M. Showalter foundation (to A. H.).
[S] This article contains supplemental Figs. S1–S4.
[1] Both authors contributed equally to this work.
[2] To whom correspondence may be addressed: Dept. of Pharmacology, University of California, Davis, 451 Health Science Dr., Davis, CA 95616. Tel.: 530-752-6517; Fax: 530-752-7710; E-mail: dmbers@ucdavis.edu.
[3] To whom correspondence may be addressed: Stark Neurosciences Research Institute, Indiana University School of Medicine, 950 W. Walnut St., R2-480, Indianapolis, IN 46202. Tel.: 317-278-8513; Fax: 317-278-5849; E-mail: ahudmon@iupui.edu.
[4] The abbreviations used are: I_{Na}, Na^+ current; CaM, calmodulin; CaMKII, Ca^{2+}/calmodulin-dependent protein kinase II; ANOVA, analysis of variance; AIP, autoinhibitory peptide.

which are loss-of-function effects, consistent with Brugada syndrome (8). In addition, CaMKII increases late or persistent I_{Na}, which has also been reported in stressed myocytes and in heart failure (9) and resembles long QT syndrome. These effects were blocked by acute CaMKII inhibition, confirming that CaMKII-dependent phosphorylation is involved. Because CaMKII is up-regulated in heart failure and can modulate $Na_V1.5$, understanding its mechanism of action is essential to understanding the physiology and pathophysiology of I_{Na} gating.

Here, we sought to identify the molecular target of CaMKII-dependent regulation of I_{Na}. Biochemical approaches were used to identify sites at which CaMKII phosphorylates $Na_V1.5$, and whole cell patch clamp recordings of wild-type (WT), non-phosphorylatable, and phosphomimetic mutant $Na_V1.5$ were used to test for CaMKII-induced I_{Na} gating changes.

EXPERIMENTAL PROCEDURES

Recombinant CaMKII—α-CaMKII was expressed using a baculoviral expression system in insect cells and purified as described previously (10, 11). δ_C-CaMKII (expressed with a His_6 tag in the baculoviral expression system) was applied to Ni^+-NTA-agarose and eluted using an imidazole gradient (0–1 M). Fractions containing the kinase were then added to a CaM-Sepharose column in the presence of 50 mM HEPES, pH 7.4, 0.1 mM EDTA, and 2 mM $CaCl_2$, washed, and eluted in 50 mM HEPES, pH 7.4, 400 mM NaCl, 0.1 mM EDTA, and 10 mM EGTA. A final gel filtration column purification step was performed as described previously (10, 11). Monomeric δ_C-CaMKII (δ_C-$CaMKII_{mono}$) with an intein fusion tag was expressed in Rosetta2 DE3 bacteria, lysed, and enriched using a chitin affinity column. The kinase was eluted in 50 mM HEPES, pH 7.4, 0.1 mM EDTA, and 50 mM DTT and subsequently applied to a CaM-Sepharose column/gel filtration column as described above for δ_C-CaMKII.

CaMKII Phosphorylation of $Na_V1.5$—For $Na_V1.5$-stably expressing HEK293 cell lysates, 10-cm dishes were lysed in 20 mM Tris, pH 7.4, 200 mM NaCl, 0.1 mM EDTA, and 1% Triton X-100, and $Na_V1.5$ was immunoprecipitated using polyclonal $Na_V1.5$ antibody (Alomone, catalog no. ASC-005) and protein A/G-agarose. The immunoprecipitated proteins were extensively washed in lysis buffer, and the immunoprecipitates were phosphorylated with 1 μg of α-CaMKII in reaction mix (50 mM HEPES, pH 7.4, 100 mM NaCl, 10 mM $MgCl_2$, 100 μM ATP, 2 mM $CaCl_2$, 5 μM CaM, and [γ-^{32}P]ATP (10 μCi/reaction) (12). After a 4-min incubation at 30 °C, the reaction was quenched with 50 mM Tris, pH 7.4, and 50 mM EDTA in phosphate-buffered saline. Immobilized proteins were collected by centrifugation, and the reaction mix was removed and extensively washed in quenching buffer. Immobilized proteins were solubilized in 4× LDS sample buffer and β-mercaptoethanol. Following gel electrophoresis, Western blotting was performed using monoclonal pan-Na_V antibody (Sigma, catalog no. S8809) and $Alexa_{680}$ goat anti-mouse secondary. The immunoprecipitated $Na_V1.5$ protein was visualized using a LI-COR/Odyssey version 3.0 imaging station, and the phosphorylated proteins were visualized using autoradiography.

CaMKII Phosphorylation of GST-Proteins and Soluble Peptides—GST-tagged intracellular regions of $Na_V1.5$ (N terminus, L1–L3, and C terminus) as well as GST-tagged mutants of the L1 were expressed in Bl-21 cells overnight at 16 °C using 0.1 mM isopropyl 1-thio-β-D-galactopyranoside. Cell pellets were lysed in lysis buffer (20 mM Tris, pH 7.4, 200 mM NaCl, 0.1 mM EDTA, and 2× protease inhibitors (Calbiochem, catalog no. 539137)), and GST fusion proteins were bound to glutathione beads in binding buffer (20 mM Tris, pH 7.4, 200 mM NaCl, 1 mM EDTA, and 0.1% Tween 20) for 2 h at 4 °C (12, 13). Following binding, beads were extensively washed (in binding buffer) to remove any unbound lysate. GST-bound fragments were then phosphorylated with 25 ng of δ_C-CaMKII in reaction mix (see above). δ_C-$CaMKII_{mono}$ was substituted for δ_C-CaMKII in Fig. 3, *E* and *F*, to avoid potential contaminating quantification of L1 phosphorylation with autophosphorylated δ_C-CaMKII. After incubation (1 min to 3 h), the reaction was quenched with 50 mM Tris, pH 7.4, and 50 mM EDTA in PBS, beads were extensively washed, and protein fragments were solubilized and denatured using 2× LDS sample buffer with β-mercaptoethanol at 70 °C. Radioactivity of phosphorylated proteins was detected directly on the beads using scintillation counting as described previously (13). Gel electrophoresis followed by Coomassie staining allowed for the visualization of GST fusions. CaMKII phosphorylation of GST fusions was visualized in the gel with autoradiography or phosphorimaging using MultiGauge version 3.0. Soluble peptides from different regions of the intracellular loop 1 (control, EEQNQATIAETEEKE; 483/484, KRRKRMSSGTEECGE; 516, NHLSLTRGLSRTSMK; 571, LRRTSAQGQPSPGTS; 593/594, LHGKKNSTVDCNGVV; and 571*, LLVPWPLRRTSAQGQ) were purchased from New England Peptide (Gardner, MA) or synthesized/HPLC-purified and reconstituted in dimethyl sulfoxide. For soluble peptide experiments, δ_C-CaMKII (25 ng) was incubated with the same reaction mix listed above and 100 μM (or 500 μM) peptide of interest for 1 min to 1 h at 30 °C. The solution was then transferred to P-81 filter papers (Whatman, GE Healthcare), washed with 75 mM phosphoric acid, and counted in a Beckman β-counter. The purified α-CaMKII, δ_C-CaMKII, and δ_C-$CaMKII_{mono}$ all had specific activity of 4–15 μmol/min/mg, as determined using the peptide AC-2 as a substrate. Statistical analysis of phosphorylation was performed using a one-way ANOVA with post hoc Dunnett's test with a statistical significance accepted at $p < 0.05$. To determine the stoichiometry of peptide phosphorylation, 100 μM peptide (483/484, 516, 571, and 593/594) was phosphorylated *in vitro* by 25 ng of δ_C-CaMKII as described above for 3 h. Using the ATP concentration, specific activity of the *in vitro* kinase assay, and the known peptide concentrations, the moles of phosphate/mole of peptide was calculated. To determine the stoichiometry of GST-L1 fragment phosphorylation, protein levels in the Coomassie-stained ~58 kDa band corresponding to full-length GST-L1 were quantified using LI-COR/Odyssey version 3.0. The concentration of GST-L1 protein was quantified against a standard curve of BSA (60 kDa; linear from 0.5 to 10 μg). The moles of GST-L1 were then calculated using the determined concentration and the expected molecular mass of full-length GST-L1 (58.8 kDa). The full-length GST-L1 band

was then cut out, and ^{32}P incorporation in the band was quantified using Cerenkov counting in a scintillation counter. Using the ATP concentration and specific activity of the reaction, the moles of ATP/GST-L1 band were calculated and compared with the moles of protein.

CaMKII Co-immunoprecipitation with $Na_V1.5$—HEK293 cells were transfected with $hNa_V1.5$ and GFP-δ_C-CaMKII using Lipofectamine 2000. Following a 48-h incubation, the transfected cells were lysed in lysis buffer (see above), centrifuged (14,000 × *g* at 4 °C for 30 min), and precleared with Protein A- and G-agarose. GFP-CaMKII was immunoprecipitated with monoclonal GFP antibody (Clontech, catalog no. 632375). Mouse IgG was used as a control. Primary antibodies were pulled down using Protein G-agarose. The agarose was washed repeatedly using lysis buffer, and the agarose-bound proteins were solubilized in 4× LDS sample buffer and β-mercaptoethanol. Following gel electrophoresis and transfer, parallel Western blotting was performed using monoclonal GFP and monoclonal pan-Na_V antibodies. The proteins were detected using a $DyLight_{800}$ goat anti-mouse secondary antibody and visualized using a LI-COR/Odyssey version 3.0 imaging station.

CaMKII Targeting to L1 Domain of $Na_V1.5$—GST-tagged intracellular regions of $Na_V1.5$ (N terminus, L1–L3, and C terminus) were bound to glutathione-Sepharose as described (12, 13). Prior to the application of CaMKII, the immobilized proteins on the Sepharose beads were blocked in binding buffer with the addition of 5% BSA. Purified δ_C-CaMKII (1 μg total (unlabeled and $DyLight_{800}$-labeled; 3:1 ratio)) was then bound to the beads for 1 h at 4 °C. To ensure that CaMKII concentration was not limited in assays determining the stoichiometry of binding to GST-L1, 20 μg of unlabeled kinase was added to the reaction. For treatment groups with naive CaMKII, δ_C-CaMKII was diluted in 50 mM HEPES, pH 7.4, and 1 mM EGTA for 2 min on ice prior to the addition to the binding reaction. For treatment groups with autophosphorylated CaMKII, δ_C-CaMKII was incubated in 50 mM HEPES, pH 7.4, 0.5 mM $CaCl_2$, 5 μM CaM, 5 mM $MgCl_2$, and 1 mM ATP for 2 min on ice and was subsequently added to the binding reactions. Following incubation with δ_C-CaMKII, the beads were then extensively washed. The beads were then applied to an *in vitro* CaMKII assay with 20 mM HEPES, pH 7.4, 100 mM NaCl, 2 mM $CaCl_2$, 5 μM CaM, 10 mM $MgCl_2$, 100 μM ATP, 50 μM syntide-2, and 6 μCi/reaction [γ-^{32}P]ATP for 3 min at 30 °C (12). ^{32}P incorporation on syntide-2 was assessed using a Beckman β-counter after transferring the solution to P-81 filter papers and washing unincorporated ^{32}P with 75 mM phosphoric acid. CaMKII binding was also visualized using a LI-COR imaging station to detect $DyLight_{800}$-labeled CaMKII in the Coomassie-stained electrophoretic gel. Student's *t* test was performed for statistical comparison with significance accepted at $p < 0.05$. Stoichiometry of binding was assessed by quantifying protein levels of GST-L1 and δ_C-CaMKII in the Coomassie-stained gel using LI-COR/Odyssey version 3.0 analysis software. The protein bands at 52 kDa (CaMKII subunit) and 58 kDa (GST-L1) were compared with a standard curve of increasing amounts of δ_C-CaMKII (linear from 0.5 to 10 μg). This allowed for the determination of each protein concentration. Using this concentration and the predicted molecular weight of each protein, the moles of CaMKII and GST-L1 were calculated.

Peptide SPOTS Arrays—Peptide arrays were constructed using the SPOTS synthesis method (11). Following synthesis, the peptide membrane is blocked at 4 °C overnight in binding buffer plus 5% BSA. δ_C-CaMKII (~34 nM) was added to 50 mM HEPES, pH 7.4, 100 mM NaCl, 10 mM $MgCl_2$, 100 μM ATP, 2 mM $CaCl_2$, 5 μM CaM, 3 μCi/ml [γ-^{32}P]ATP. The reaction was incubated for 5 min at room temperature, washed in 75 mM phosphoric acid three times, and visualized using phosphorimaging (Fuji phosphor imager). Phosphorylation of each peptide spot was detected and quantified using MultiGauge version 3.0. Statistical comparison was by one-way ANOVA with post hoc Dunnett's test.

Transfection—Electrophysiological recordings were performed in HEK293 cells (Invitrogen, catalog no. 70507), which provide a well controlled environment to study the direct influence CaMKII activity has on channel function. The HEK293 cells were cultured in DMEM supplemented with 10% FBS and 5% penicillin/streptomycin and passaged to maintain them subconfluent (maximum of 20 passages). One day before transfection, cells were plated on 35 × 50-mm coverslips adapted for electrophysiology. They were transfected using Lipofectamine 2000 (0.5 μl/cm^2) in Opti-MEM (Invitrogen) per the manufacturer's instructions, with plasmids ($hNa_V1.5$ WT or mutant, in all cases with the C373S mutation to reduce tetrodotoxin sensitivity) and, where indicated, GFP-δ_C-CaMKII, all at 0.5 μg/cm^2) for 5–6 h and then washed and incubated for at least 24–36 h before experiments. This overexpression within our reduced system mimics physiological disease states, such as heart failure, which exhibit increased CaMKII expression and activity (4–7). Cells that were visibly fluorescent were identified as expressing δ_C-CaMKII. For all experiments, single cells expressing $Na_V1.5$ were selected based on their appearance and on the presence of I_{Na} without secondary artifacts.

Solutions for Electrophysiology—Pipette solutions and recording protocols were standard for Na^+ channel electrophysiology as described previously (8). Cells were bathed in Tyrode solution consisting of 140 mM NaCl, 1 mM $MgCl_2$, and 0.5 mM $CaCl_2$ (to help maintain stable pipette seals), with 4 mM CsCl substituted for KCl. The base pipette solution contained 10 mM NaCl, 50 mM CsCl, 90 mM cesium glutamate, 5 mM Tris-ATP, 0.3 mM Li-GTP, 5 mM Cs_4-1,2-bis(2-aminophenoxy)ethane-*N*,*N*,*N*′,*N*′-tetraacetic acid, and 10 mM HEPES, titrated to pH 7.2 with CsOH at room temperature. All pipette solutions contained 1 μM calmodulin (Calbiochem/EMD, catalog no. 208690). $CaCl_2$ and $MgCl_2$ were added to yield 1 mM free [Mg^{2+}] and 1 μM free [Ca^{2+}] (high Ca^{2+} condition in all experiments here) or, in preliminary studies, <100 nM free [Ca^{2+}] (low Ca^{2+}; calculated by MaxChelator). To inhibit CaMKII in select experiments, 1 μM AIP was added to pipette solution. Notably, AIP substantially lower than 1 μM did not unambiguously block δ_C-CaMKII responses. Pipette and bath solutions were designed with closely matching osmolarity, which stabilized pipette access and improved longevity of recording. All pipette solutions were stored frozen at −80 °C in 500-μl single-use aliquots. Fluoride was not used in the solutions.

Electrophysiological Recording—Whole cell I_{Na} was recorded using ruptured patch voltage clamp at room temperature, with an Axopatch 200B amplifier, 1322A interface, and pClamp 8.2 software (Molecular Devices). Seal resistance for successfully recorded cells was typically >5 gigaohms, and uncompensated on-cell access resistance ranged from 1 to 4 megaohms. Pipettes were made from either type 7052 or 8250 glass, were thin-walled and broadly tapered to promote diffusion, and were heat-polished. After patch rupture, 2 min was allowed for diffusion, at which time each cell was checked for expression of I_{Na}. Records used experimentally were recorded ≥4 min postrupture, and where possible the order of protocols was standardized to limit possible implicit time dependence. A liquid junction potential between pipette and bath solutions, −9 mV, pipette-negative, originated due to substitution of glutamate for most of the chloride in the pipette solution, and was corrected during recording. Capacitance transients due to pipette and cell membrane were cancelled, and series (access) resistance was compensated to >70%. The quality of transient cancellation and clamp compensation was continuously monitored except during the actual acquisition of data.

Electrophysiological Protocols—At the start of each protocol as well as between episodes, Na^+ channels were held at −140 mV, promoting initial rest and subsequent return to the fully available closed state. During intervals between protocols, cells were held at −110 mV to promote longer experimental life.

To establish activation voltage dependence, the current-voltage relation was recorded. Cells were step-depolarized for 50 ms to test potentials between −80 and +30 mV. To measure steady state inactivation voltage dependence, cells were predepolarized for 500 ms to potentials between −140 and −20 mV. The extent of inactivation was measured immediately after the prepulse by applying a −20 mV depolarization for 50 ms. After each test pulse, 140 ms was allowed at −140 mV for recovery, followed by a second −20 mV pulse, which provided a full availability reference current for the particular trace.

Time-dependent properties were measured as follows. Decay of current after its peak at −30 mV during the above current-voltage protocol was used to measure the rate of fast inactivation. Recovery from fast inactivation was studied by applying a 50-ms pulse to −20 mV, which initialized maximal fast inactivation. Recovery after increasing intervals at −140 mV (duration range 0.5–128 ms) was measured by a second pulse to −20 mV. Peak I_{Na} recorded during the initial pulse served as a reference for fractional recovery in each episode. I_{Na} decay was fit well by a biexponential function (τ_1 0.736 ± 0.16 and τ_2 2.3 ± 0.16 ms (S.D.) with 89% in the faster component; $n = 28$) and did not differ among $Na_V1.5$ mutants or with/without AIP. Recovery from fast inactivation was also biexponential ($\tau_1 = 2.98 \pm 1.04$, $\tau_2 = 149 \pm 182$ ms (S.D.), with 89% in the faster component; $n = 8$) and did not differ among $Na_V1.5$ mutants or with/without AIP.

To measure the rate and extent of entry into intermediate and slow inactivated states, pulses at −20 mV were applied for 5 ms to 4.75 s, and recovery at −140 mV was allowed for 20 ms to allow full recovery from rapid inactivation (see "Results"), after which a test pulse at −20 mV was applied. In this protocol, the peak current during the initial inactivating pulse provided a reference against which the ensuing inactivation was measured. Corresponding with the recovery from fast inactivation protocol, recovery from intermediate and slow inactivation was measured using a 3-s inactivating prepulse at −20 mV (shown to be effective at inducing slow inactivation; see "Results"), after which recovery at −140 mV was allowed for durations from 0.5 ms to 3 s. This protocol was preceded and followed by separate reference depolarizations to −20 mV applied under full availability conditions.

Voltage step and time interval sequences in the above protocols were chosen for efficiency. Increments were adjusted to concentrate data in the voltage or time ranges expected to show the most variation, and the total number of episodes was chosen sufficient for robust curve fitting without requiring undue experimental time.

Electrophysiological Analysis—All records were corrected for passive leak. Average current measured during a −140 mV interval (usually the beginning) within each episode when I_{Na} was assuredly not active was expressed as a point estimate of conductance ($G_{leak} = I_{leak} \times V_{hold}$) which was then used to infer and subtract leak current at each time and voltage during the rest of the episode.

Activation voltage dependence was used to screen cells for technical errors that would preclude further analysis. In records with good voltage control (based on the slope of the activation curve), we found that half-activation voltage did not differ significantly among transfects or treatments (see "Results"). Leak-corrected peak current *versus* voltage data were parameterized using the Boltzmann equation,

$$I_{Na} = (G_{max}/(1 + \exp((V_{50} - V_m)/k)))(V_m - E_{rev}) \quad \text{(Eq. 1)}$$

in which G_{max} is the maximum conductance, V_{50} is the half-activation voltage, V_m is the test potential, k is the slope of voltage dependence, and E_{rev} is the current reversal potential. Similarly, the steady state inactivation voltage dependence (availability curve) was found by fitting the following,

$$I_{Na} = I_{max}/(1 + \exp((V_m - V_{50})/k)) \quad \text{(Eq. 2)}$$

where I_{max} is a surrogate for G_{max} because test V_m is constant in the inactivation protocol. Time dependences were fit by either decreasing the following,

$$I(t) = I_{peak}\,(w \exp((t - t_{peak})/\tau_1) + (1 - w)\exp((t - t_{peak})/\tau_2)) + C \quad \text{(Eq. 3)}$$

or increasing the following,

$$I(t) = I_{peak}\,(1 - (w \exp((t - t_{peak})/\tau_1) + (1 - w)\exp((t - t_{peak})/\tau_2))) + C \quad \text{(Eq. 4)}$$

biexponential functions, where I_{peak} and t_{peak} were measured directly from records, and w (weight; $0 < w < 1$), τ_1 and τ_2 (time constants), and C (asymptotic value) were fit. In some analyses, C or w was constrained to 0, or a plateau was included before a single decreasing exponential.

Preliminary I_{Na} experiments under several conditions (pipette solutions with and without AIP and low *versus* high

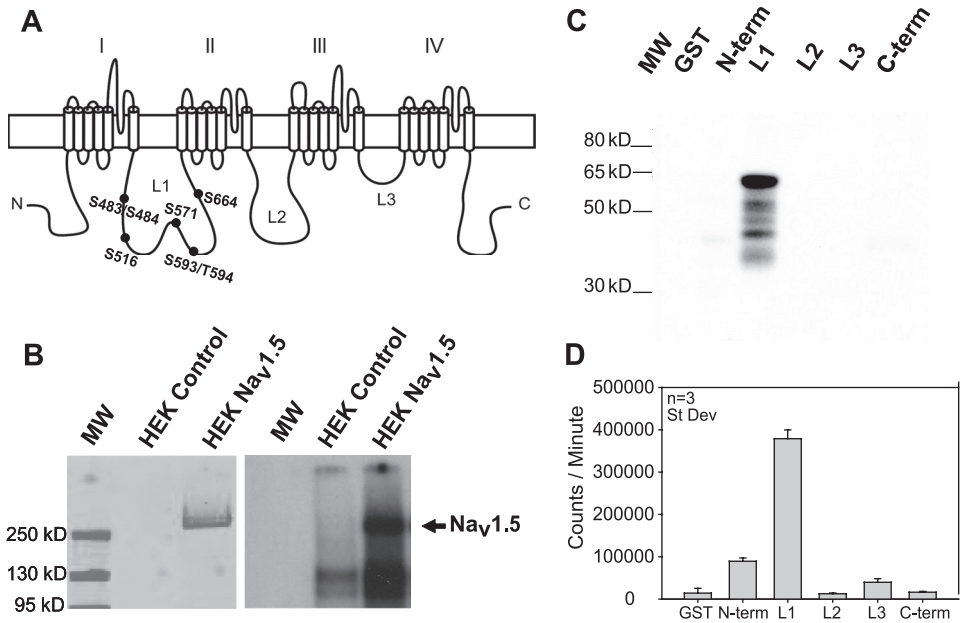

FIGURE 1. **CaMKII phosphorylates L1 of $Na_V1.5$.** *A*, human $Na_V1.5$ has five major intracellular regions (N and C termini plus loops 1–3 (L1–L3). Potential CaMKII phosphorylation sites in the L1 are *highlighted*. Single-letter amino acid codes are shown. *B*, $hNa_V1.5$ immunoprecipitated from HEK293 cells was exposed to activated α-CaMKII with [γ-^{32}P]ATP. Western blot (*left*) indicates $hNa_V1.5$ in stably expressing HEK293 cells, and the autoradiogram (*right*) indicates phosphorylation at $Na_V1.5$ molecular weight. *C* and *D*, bacterially expressed GST fusion proteins of intracellular $hNa_V1.5$ regions were exposed to activated δ_C-CaMKII with [γ-^{32}P]ATP. *C*, autoradiograph indicates phosphorylation of the L1 after δ_C-CaMKII phosphorylation. *D*, average ^{32}P incorporation ($n = 3$, ±S.D. (*error bars*)) of GST fusion proteins detected following Cerenkov counting.

Ca^{2+}, transfection of $hNa_V1.5$ ± GFP-δ_C-CaMKII) were used to optimize detection of CaMKII effects (supplemental Fig. S3). All data reported here were recorded with GFP-δ_C-CaMKII and $hNa_V1.5$ co-transfected and with pipette solutions containing 1 μM CaM and 1 μM free Ca^{2+} ± 1 μM AIP unless noted otherwise. All data were processed and parameterized for statistical treatment using home-written Microsoft Visual Basic scripts run with Microsoft Excel. We analyzed parameterized data when appropriate with unpaired Student's *t* tests and one-way or two-way ANOVA followed by post hoc Tukey test for all pairwise comparisons, using the $Na_V1.5$ isoform and the presence of AIP as factors, using GraphPad Prism software, version 5.02 for Windows (GraphPad Software, San Diego, CA).

RESULTS

Identification of CaMKII Phosphorylation Sites on $Na_V1.5$—Sodium channels are multiprotein complexes. The α-subunit (*e.g.* $Na_V1.5$) contains the channel pore and major determinants of gating and drug binding. These large transmembrane proteins (>220 kDa) contain four domains (*I–IV* in Fig. 1*A*), each containing six α-helical transmembrane segments, with a voltage sensor and a pore loop. The $Na_V1.5$ α-subunit has intracellular N and C termini, plus three major intracellular loops connecting domains I–IV, termed L1–L3, respectively (Fig. 1*A*). When we express human $Na_V1.5$ in HEK293 cells, it is a substrate for recombinant rat α-CaMKII, based on ^{32}P incorporation (Fig. 1*B*), similar to rodent $Na_V1.5$ immunoprecipitated from heart (8). No CaMKII phosphorylation is observed in untransfected HEK293 cells at the molecular weight for $Na_V1.5$. To narrow down the CaMKII phosphorylation site(s), we constructed GST fusions of the major cytoplasmic regions of $hNa_V1.5$ (L1–L3 and the N and C termini). Bacterially expressed GST fusion proteins were purified and phosphorylated directly on glutathione-Sepharose by recombinant human δ_C-CaMKII (the predominant cytoplasmic cardiac isoform). Relative expression patterns for these GST fusion proteins are shown in the Coomassie-stained gel in supplemental Fig. S1*A* (which also shows the predicted molecular weight for each fusion protein). CaMKII phosphorylation assessed by ^{32}P incorporation and autoradiography was limited primarily to the L1 region of $Na_V1.5$, as illustrated by the autoradiographic image (Fig. 1*C*) and quantified data (Fig. 1*D*); the L1 domain is reproducibly the best CaMKII substrate tested under these conditions. When phosphorylation of the GST-tagged intracellular regions is normalized to the protein expression level of the predicted molecular weight for each fusion protein, the L1 is still the predominant CaMKII substrate (supplemental Fig. S1*B*). An estimated 1.59 ± 0.10 mol of phosphate were incorporated/mol of GST-L1, suggesting that there is more than one phosphoacceptor site per full-length L1. These data are in good agreement with recent reports using a similar strategy to confirm L1 as a CaMKII phosphorylation hot spot (14, 15).

CaMKII Binding to L1—The proximity of protein kinases to their substrates is important for the timing and specificity of signal transduction (16). CaMKII was previously shown to coimmunoprecipitate with cardiac $Na_V1.5$ (8). We first verified these findings in HEK293 cells expressing $hNa_V1.5$ and GFP-δ_C-CaMKII. As expected, δ_C-CaMKII co-immunoprecipitated with $hNa_V1.5$ (Fig. 2*A*). No GFP-δ_C-CaMKII or $hNa_V1.5$ were detected when pulled down with an IgG control (Fig. 2*A*). Next, we aimed to identify which intracellular domain of $Na_V1.5$ (N terminus, L1–L3, and C terminus) stably interacted with CaMKII. For this, δ_C-CaMKII (naive, in the presence of Ca^{2+}/

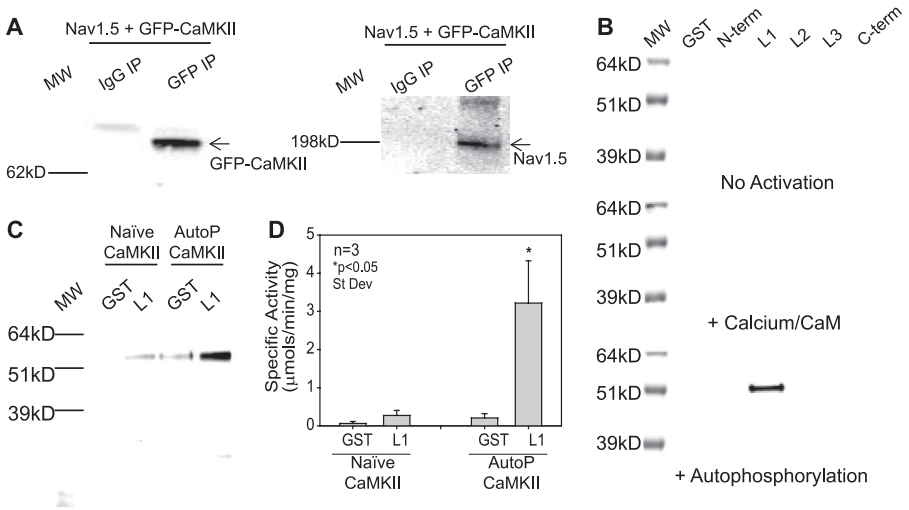

FIGURE 2. **Autophosphorylated CaMKII tethers to L1 of $Na_V1.5$.** *A*, HEK293 cells expressing hNaV1.5 and GFP-δ_C-CaMKII were lysed, pulled down with monoclonal GFP antibody, and subsequently blotted for GFP-δ_C-CaMKII (*right*) and $hNa_V1.5$ (*left*). Full-length $hNa_V1.5$ co-immunoprecipitated (*IP*) with GFP-δ_C-CaMKII. *B*, Western blot detection of δ_C-CaMKII bound to GST-tagged fragments of the major intracellular loops of $hNa_V1.5$ under naive conditions (*top*), in the presence of Ca^{2+}/CaM (*middle*), and when δ_C-CaMKII was preautophosphorylated (*bottom*). *C*, image of 1 μg of Ca^{2+}/CaM/autophosphorylated $DyLight_{800}$-labeled δ_C-CaMKII bound to GST-L1 and not GST alone (*right lanes*). Naive δ_C-CaMKII (*left lanes*) did not bind GST-L1. *D*, average phosphorylation ($n = 3$, $\pm$ S.D. (*error bars*)) of syntide-2 with GST-L1 pull-down fragments bound to autophosphorylated δ_C-CaMKII (*right bars*) and not naive CaMKII (*left bars*). Data are represented as specific activity with 1 μg of multimeric human δ_C-CaMKII. *, significant difference compared with GST alone ($p < 0.05$; *t* test).

CaM, and autophosphorylated) was applied to beads bound with GST-tagged intracellular fragments or GST alone as described previously (11, 12). Gel electrophoresis with Western blot detection of CaMKII indicated that autophosphorylated CaMKII preferentially targets to GST-L1 (Fig. 2*B*). This finding was verified using $DyLight_{800}$-labeled δ_C-CaMKII. Fluorescent detection of CaMKII indicated that autophosphorylated CaMKII forms a stable interaction with the first major intracellular loop of $Na_V1.5$ (Fig. 2*C*; for full Coomassie-stained gel, see supplemental Fig. S2A). There was appreciably less binding when naive CaMKII (non-activated) was incubated with either GST or GST-L1, suggesting that, analogous to other ion channels and accessory proteins (12, 17–19), CaMKII activation exposes a targeting site for interacting with the L1 domain of $hNa_V1.5$. The stoichiometry of CaMKII binding was 0.92 $\pm$ 0.11 mol of kinase subunit (52 kDa)/mol of full-length GST-L1. The binding of CaMKII to L1 was also quantified using an *in vitro* kinase assay (12, 13). In this assay, an increase in syntide-2 phosphorylation is associated with CaMKII binding to a target protein. A significant increase in syntide-2 phosphorylation was only observed when autophosphorylated CaMKII was incubated with and allowed to bind GST-L1 (Fig. 2*D*). These data demonstrate for the first time that activated CaMKII forms a stable interaction with the L1 domain of $Na_V1.5$.

Identification of CaMKII Phosphorylation Sites in L1—There are seven consensus CaMKII phosphorylation sites in five regions of L1 conforming to Arg/Lys-*X*-*X*-Ser/Thr (20) (Fig. 1*A*). However, CaMKII can also phosphorylate non-canonical phosphorylation motifs (21). Therefore, we experimentally scanned the entire L1 domain for potential CaMKII phosphorylation sites using a non-biased overlapping peptide array. A total of 141 peptides were constructed using a robotic peptide synthesizer (Intavis, MultiPep). Each peptide is 15 amino acids in length, and tiled peptides are shifted by two amino acids (13 overlapping amino acids per peptide). Thus, each potential CaMKII phosphorylation motif is represented within multiple peptides, creating several opportunities for the Ser/Thr residues to be phosphorylated as they move in and out of a family of overlapping peptides. These immobilized peptides are synthesized on a modified cellulose membrane using routine Fmoc (*N*-(9-fluorenyl)methoxycarbonyl) chemistry (22, 23). Activated δ_C-CaMKII was applied to the immobilized peptides (11) in the presence of [γ-^{32}P]ATP. Phosphorylated peptides were imaged on autoradiographic film (Fig. 3*A*) and quantified using phosphorimaging (Fig. 3*B*). In this non-biased strategy, several overlapping peptide motifs were phosphorylated, including Ser-483/Ser-484, Ser-516, and Ser-593/Thr-594 (Fig. 3, *A* and *B*). Our *in vitro* phosphorylation approach did not recognize Ser-571, a site recently reported to be a CaMKII substrate on $Na_V1.5$ (15).

We further investigated the potential CaMKII phosphorylation sites identified in the immobilized peptide array using soluble peptides (Fig. 3*C*). For comparison, a peptide containing Ser-571 was also included. Using this assay, only soluble peptides encompassing the region around Ser-516 and Ser-593/Thr-594 exhibited significantly greater ^{32}P incorporation than a control peptide (encompassing residues 417–431 of the L1 domain) (Fig. 3*C*). The stoichiometry of this phosphorylation following a 3-h incubation was 1.18 $\pm$ 0.12 mol of phosphate/mol of Ser-516 peptide and 0.44 $\pm$ 0.01 mol of phosphate/mol of Ser-593/Thr-594 peptide. These data suggest that the Ser-516 peptide is a better CaMKII substrate; however, it is also conceivable that the reduced stoichiometry displayed by the 593/594 peptide is due to a Cys residue forming disulfide bonds between peptides. We did not observe significant phosphorylation over background for a soluble peptide harboring the Ser-483/Ser-484 motif (0.01 mol of phosphate/mol of peptide), consistent with previous work showing that this region was not important for CaMKII regulation of $Na_V1.5$ (15). Although we do not fully understand this discrepancy, it is conceivable that

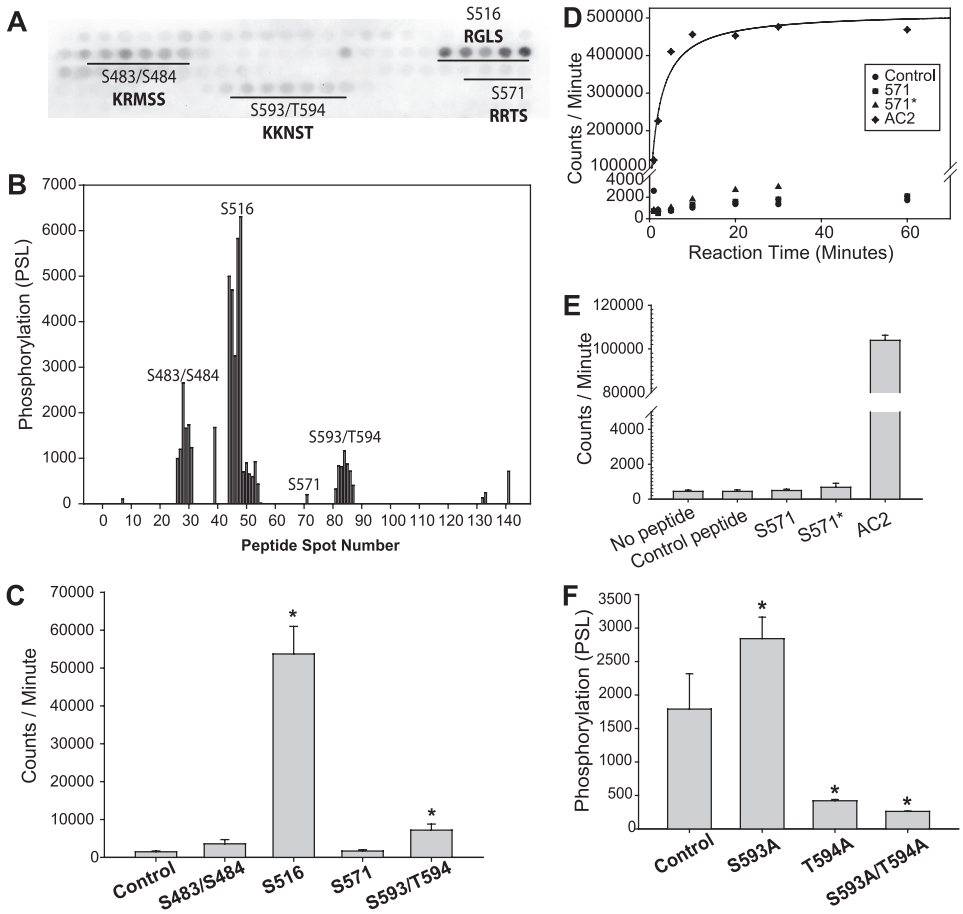

FIGURE 3. **CaMKII phosphorylates Ser-516 and Ser-593/Thr-594 in L1.** *A*, phosphor image of immobilized tiled peptide array of L1 after δ_C-CaMKII phosphorylation with [γ-^{32}P]ATP (*darkness* indicates ^{32}P incorporation on that peptide). Single-letter amino acid codes are shown. *B*, phosphorylation intensity of each peptide spot in *A*, detected using MultiGauge version 3.0. *C*, soluble peptide (50 μM) phosphorylation by monomeric δ_C-CaMKII ($n = 3$, $\pm$S.D. (*error bars*); *, $p < 0.05$ *versus* control peptide). 15-mers were centered near the indicated sites. *D*, time course of monomeric δ_C-CaMKII phosphorylation of 500 μM control peptide, original unbiased Ser-571 peptide, the biased 571* peptide (see "Experimental Procedures" for sequence), and 50 μM AC2, a known CaMKII substrate. *E*, average phosphorylation ($n = 3$, $\pm$S.D.) of soluble peptides in *D* at the 1 min time point. *F*, average phosphorylation ($n = 3$, $\pm$S.D.) of immobilized peptides with wild-type control, as well as Ser-593/Thr-594 single point Ala mutations and a double-point Ala mutation. S593A/T594A and T594A exhibit decreased phosphorylation compared with wild-type control ($n = 3$, $\pm$S.D.; *, $p < 0.05$ *versus* control Ser-493/Thr-494; one-way ANOVA, post hoc Dunnett's test).

the Ser-483/Ser-484 motif is picked up as a substrate using the immobilized assay because multivalent proteins bind to immobilized peptides with a much higher affinity on a two-dimensional surface (24). As observed with immobilized peptides, a soluble peptide containing the Ser-571 motif was again not phosphorylated above background (Fig. 3*C*), with only 0.02 mol of phosphate incorporated/mol of peptide. However, in this Ser-571 peptide, the phosphorylation site was located toward the N-terminal end of the peptide (as derived from the unbiased immobilized array; see "Experimental Procedures" for sequences). Because it was possible that this unbiased approach resulted in a peptide that was missing a component of the CaMKII targeting sequence, another peptide with the Ser-571 phosphorylation site at the center of the sequence was generated, termed 571*. Similar to the original Ser-571 peptide, 571* was not a CaMKII substrate *in vitro* even when incubation was extended from 1 to 60 min or when the working peptide concentration was increased to 500 μM (Fig. 3, *D* and *E*). Thus, Ser-571 is not phosphorylated by CaMKII *in vitro*.

To identify the contribution of Ser-593 *versus* Thr-594 as the CaMKII phosphoacceptor site, immobilized peptides with point mutations of each site individually as well as in combination were generated and phosphorylated with δ-CaMKII. This revealed that Thr-594 is the preferential CaMKII target in peptides containing both Ser-593 and Thr-594 (Fig. 3*F*).

To examine these CaMKII substrate sequences in the context of the L1 domain, we constructed GST fusions of the full L1 domain harboring mutations of each phosphoacceptor Ser/Thr amino acid to Ala (Fig. 4, *A* and *B*). We included Ala substitutions for Ser-571 and Ser-593. The extent of phosphorylation following a 1-h incubation with δ_C-$CaMKII_{mono}$ was compared between WT L1 and each point mutation in L1 along with GST alone. Monomeric δ_C-CaMKII was used to minimize potential contamination of the ^{32}P signal in GST-L1 and its mutants with autophosphorylated CaMKII. Protein levels for each L1 fusion protein (including GST) are shown in the *upper panel* of Fig. 4*A*. Because GST is a much smaller protein (28 kDa *versus* 60 kDa for L1), a Coomassie-stained cutout is shown for this protein (the full Coomassie-stained gel is shown in supplemental Fig. S2B). An autoradiograph is shown in Fig. 4*A*, but CaMKII phosphorylation was quantified using phosphorimaging. To compensate for differences in protein expression levels and GST pull-down, each GST fusion was normalized for protein levels using LI-COR imaging of the Coomassie-stained bands.

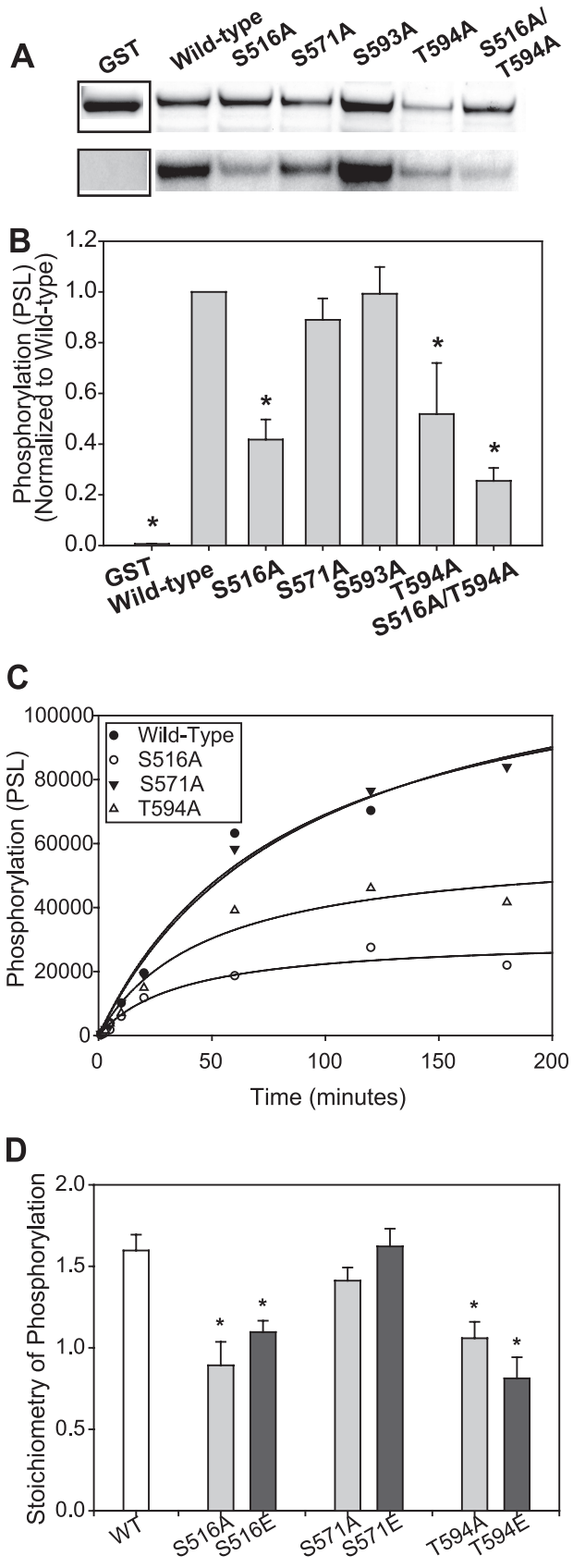

FIGURE 4. **CaMKII phosphorylation of Nav1.5 L1-GST fragments.** *A*, Coomassie stain (*top*) and phosphor image (*bottom*) of GST-tagged wild-type L1 and various L1 mutants. *B*, average phosphorylation ($n = 3$, ±S.D. (*error bars*)) of L1 constructs shown in *A*. S516A, T594A, and S516A/T594A are significantly decreased compared with wild-type GST-L1, as indicated (*, $p < 0.05$, one-way ANOVA, post hoc Dunnett's test). *C*, phosphorylation time course of GST-L1 wild-type and mutant fragments. *D*, stoichiometry of phosphorylation of GST-L1 wild-type and mutant fragments following 180-min phosphorylation by monomeric δ_C-CaMKII (time of saturation in *C*). Ala and Glu substitutions at Ser-516 and Thr-594 result in significantly decreased phosphorylation compared with wild-type and Ser-571 mutants ($n = 3$, ±S.D.; *, $p < 0.05$, one-way ANOVA, post hoc Dunnett's test).

The relative phosphorylation for each mutation normalized to WT L1 is shown in Fig. 4*B*. Compared with unconjugated GST, WT L1-GST exhibited significant phosphorylation as expected. Phosphorylation of the L1 was significantly reduced when either Ser-516 or Ser-594 was mutated to Ala (Fig. 4, *A* and *B*). The greatest reduction in phosphorylation was observed when both Ser-516 and Ser-594 were mutated in combination (S516A/S594A) (Fig. 4, *A* and *B*). Neither the S593A nor the S571A mutation reduced L1 phosphorylation significantly (Fig. 4, *A* and *B*). A full time course of GST phosphorylation up to 3 h indicated that S516A and T594A but not Ser-571 reduced phosphate incorporation in the L1 fragment (Fig. 4*C*), again indicating that Ser-516 and Thr-594, but not Ser-571, are CaMKII phosphoacceptor sites in L1. Phosphorylation of L1 with phosphomimetic (Glu) substitutions was also examined. The full time course (5 min to 3 h) of the phosphomimetic phosphorylation directly mimicked the Ala mutants shown in Fig. 4*C* (see supplemental Fig. S2*C*). As with the Ala mutants, S516E and T594E exhibited a significant reduction in phosphorylation at the 3 h time point (the point of saturation; Fig. 4*D*). This decrease was not observed with S571A or S571E. These data and the fact that the Ser-571 putative phosphorylation was not identified by the Scansite 2.0 prediction tool, even on lowest stringency (25), suggest that this sequence is not a phosphoacceptor site for CaMKII.

Electrophysiological Analysis of CaMKII Effects on WT and Mutant $Na_V1.5$ Activation—To examine functional effects of these phosphorylation sites on I_{Na}, we expressed full-length WT and mutant $hNa_V1.5$ in HEK293 cells and analyzed I_{Na} using voltage clamp. *In vitro* phosphoacceptor sites, Ser-516 and Thr-594, were mutated to non-phosphorylatable Ala or phosphomimetic Glu residues. We also tested S571A and S571E for comparison with the results of Hund *et al.* (15) and S593A. WT and Ser to Ala mutant channels were co-transfected with GFP-δ_C-CaMKII. Based on extensive preliminary studies (*e.g.* see supplemental Fig. S3), we included 1 μM free $[Ca^{2+}]$ and 1 μM CaM (to activate CaMKII) in all pipette solutions. To assess CaMKII-specific effects, we compared I_{Na} with and without the selective CaMKII peptide inhibitor AIP (1 μM) in the pipette. The presence of AIP controls for potential Ca^{2+} and CaM effects on I_{Na} and ensures that the effects measured are via CaMKII.

Representative I_{Na} traces from a holding potential (V_H) of −140 mV and I_{Na}-voltage relationship for WT, S516A, S593A/T594A, T594A, S571A, and S593A (with and without AIP) are shown in Fig. 5*A*. There was no difference in either I_{Na} amplitude or the shape of the *I*-V curves. Fig. 5, *B* and *C*, shows that CaMKII had no effect on the V_{50} of activation for any channel; nor was there any significant difference between mutant and WT channels. This agrees with results in cardiomyocytes in

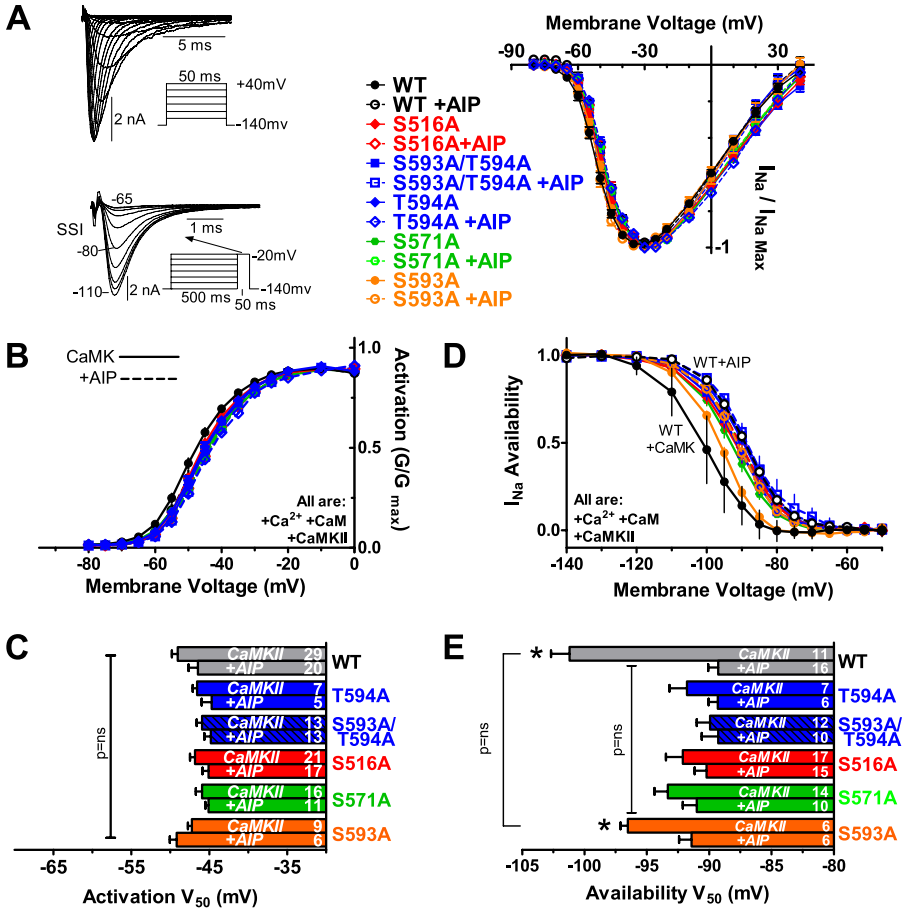

FIGURE 5. **CaMKII shifts I_{Na} availability but not activation.** I_{Na} was measured in HEK cells expressing WT, S516A, S593A/T594A, T594A, S571A, or S593A mutant $hNa_V1.5$ plus GFP-δ_C-CaMKII (pipette containing 1 μM Ca^{2+} plus 1 μM CaM with or without AIP). *A*, representative raw I_{Na} and mean current-voltage relationships. Protocols for *I*-V (*top*) and steady state inactivation (*SSI*; *bottom*) for *D* and *E* are shown. *B* and *C*, voltage dependence and V_{50} of activation were not different among groups or with/without AIP. *D* and *E*, I_{Na} availability was shifted to more negative V_m by δ_C-CaMKII in WT and S593A control, which was prevented by AIP. S516A, S593A/T594A, T594A, and S571A did not show this effect (*n* as indicated, ±S.E. (*error bars*); *, $p < 0.05$ by *t* test *versus* with AIP and two-way ANOVA but no difference among the indicated groups).

which CaMKII did not alter I_{Na} activation (8) and also shows that these mutant channels have normal WT activation.

Electrophysiological Analysis of CaMKII Effects on WT and Mutant $Na_V1.5$ Inactivation—Steady state inactivation (or availability) has been reported to be negatively shifted by CaMKII in cardiac myocytes (8). The availability of I_{Na} was measured after a 500-ms pulse to potentials between −140 and −20 mV (Fig. 5, *D* and *E*). When CaMKII was activated, there was a hyperpolarzing shift in the V_{50} for availability in both WT $Na_V1.5$ and the S593A channel (*versus* when AIP was present). Furthermore, the S593A control was not significantly different from WT under CaMKII-activating conditions. Unlike WT and S593A, the channels with Ala substitution at Ser-516, Ser-571, and Thr-594 did not display a hyperpolarizing shift upon CaMKII activation. The V_{50} of availability for phosphomutant channels was similar to that in WT channels with CaMKII blocked by AIP. Thus, mutating any one of Ser-516, Ser-571, or Thr-594 to Ala can prevent the CaMKII-dependent shift in Na^+ channel availability. The implication is that all three sites are involved in the CaMKII-dependent shift in I_{Na} availability. Preliminary studies with S483A/S484A exhibited behavior that was inconsistent with block of CaMKII-induced negative shifts in availability and was not used for further analysis.

We also tested for enhanced I_{Na} entry into intermediate inactivation (another reported effect of CaMKII on I_{Na} in cardiac myocytes) (8). Cells were depolarized to −20 mV for various times, with a subsequent 20-ms repolarization to allow recovery from fast inactivation before a test pulse (Fig. 6*A*). Fig. 6, *B* and *C*, shows that CaMKII activation in WT $Na_V1.5$ exhibits significant accumulation into intermediate inactivation, and this was inhibited by the inclusion of AIP. Like the availability shift, these changes resemble measurements in adult ventricular myocytes, where CaMKII enhanced intermediate inactivation (8). Neither S516A nor T594A with CaMKII activation exhibited as much intermediate inactivation as WT (Fig. 6*B*). Ala substitution at Ser-516, Thr-594, and Ser-571 (and double mutant at both Ser-516 and Thr-594) all prevent the CaMKII-dependent accumulation of intermediate inactivation, and with CaMKII, all are similar to WT plus AIP (Fig. 6*C*).

Phosphomimetic mutant $Na_V1.5$ channels with Glu replacing Ser-516, Thr-594, or Ser-571 or both Ser-516 and Thr-594 were used to test whether those mimic CaMKII phosphorylation effects on I_{Na}. Phosphomimetic mutants were studied without CaMKII co-transfection and with AIP in the pipette to eliminate potentially confounding effects of endogenous CaMKII phosphorylation at other sites.

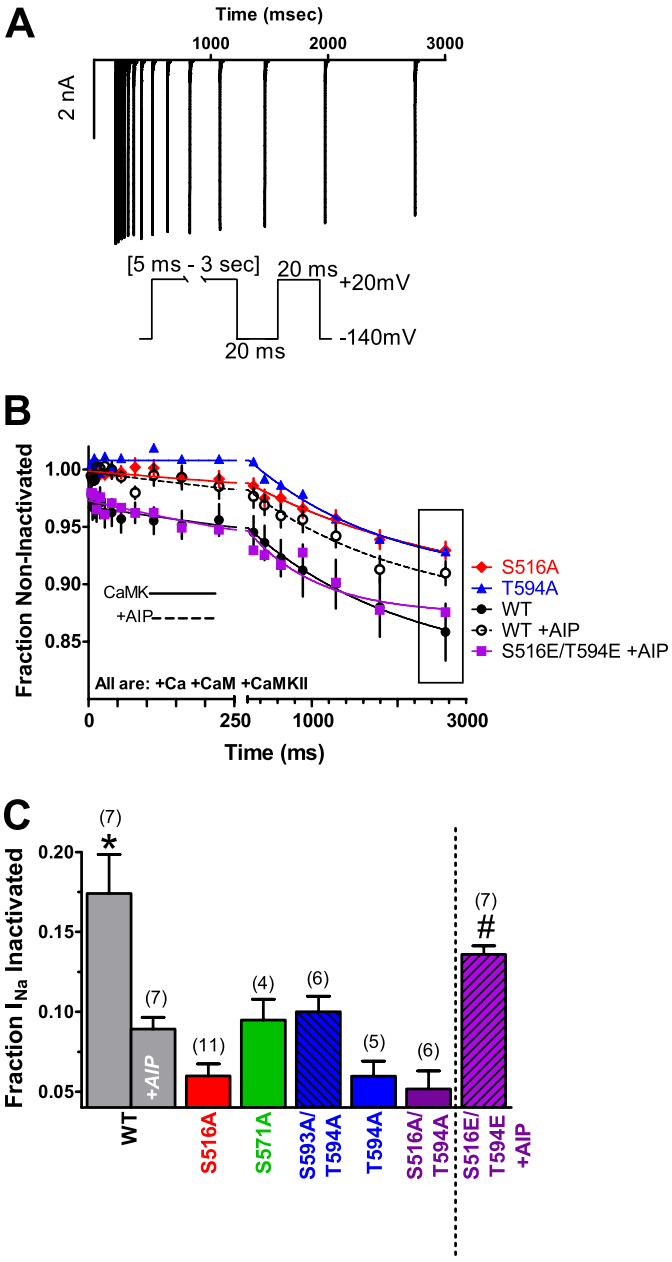

FIGURE 6. **CaMKII enhances I_{Na} entry into intermediate inactivation.** *A*, representative raw WT I_{Na} trace of enhanced entry into intermediate inactivation and two-pulse voltage protocol. *B*, time dependence of accumulation into intermediate inactivation during pulses to −20 mV was significantly greater in WT under CaMKII-activating conditions and 516E/594E phosphomimetic (+AIP) *versus* WT + AIP and phosphomutants. *C*, average accumulation of intermediate inactivation at 2.5 s from the *bounding box* in *B* (n as indicated, ±S.E. (*error bars*); *, $p < 0.05$ by ANOVA or *t* test *versus* with AIP; #, $p < 0.05$ by *t* test *versus* with AIP; p = not significant *versus* WT-AIP).

With respect to enhanced accumulation into intermediate inactivation observed for WT upon CaMKII activation, we tested the phosphomimetic channels with AIP in the pipette. No single phosphomimetic (S516E, S571E, or T594E) was able to recapitulate WT accumulation into intermediate inactivation (fraction I_{Na} inactivated at 2.5 s of 0.10 ± 0.005 (n = 3), 0.093 ±.04 (n = 4), and 0.11 ± 0.012 (n = 3) respectively). However, the S516E/T594E double phosphomimetic (+AIP) enhanced accumulation into intermediate inactivation (*versus* WT + AIP) and was not significantly different from WT with activated CaMKII. These results are consistent with multiple sites (Ser-516 and Thr-594) being involved in the CaMKII-dependent enhancement of intermediate inactivation.

We also repeated I_{Na} activation and availability measurements for S516E, T594E, S571E, and S516E/T594E channels (Fig. 7). The V_{50} of activation was again unaltered from WT in any of these mutants (Fig. 7*A*). However, the T594E and S516E mutants exhibit a strong negative shift of availability compared with WT + AIP and are not different from that seen in WT with activated CaMKII (Fig. 7*B*).

We also measured availability in phosphomimetic channels when AIP was omitted, a case where endogenous CaMKII would be active and could phosphorylate other sites (Fig. 7*C*). When AIP was omitted, T594E was not altered *versus* the AIP condition. This suggests that there is little additional CaMKII effect once Thr-594 phosphorylation is prevented. The S571E phosphomimetic did not shift with AIP present but did when CaMKII activity was allowed. That indicates that S571E could not mimic the CaMKII effect but that another available CaMKII target site (*e.g.* Thr-594) could. S516E mimics CaMKII effects in the presence of AIP, but surprisingly when CaMKII was allowed, the availability moved back toward WT + AIP. A similar availability result was seen with the S516E/T594E (with and without AIP) or the triple mutant (including S571E; Fig. 7*C*). It is possible that when Ser-516 is a Glu, either a Glu or a phosphate at Thr-594 antagonizes the functional mimic of CaMKII effects on I_{Na} availability seen with either site mutant. This indicates a complex functional interplay between these phosphorylation sites that will merit further study.

In the above studies, we also tested for the appearance of sustained or late I_{Na}, another characteristic effect of CaMKII on native cardiac I_{Na} (8, 14). We saw no evidence of late I_{Na} in any of the mutant $Na_V1.5$ channels studied; nor were the kinetics of fast inactivation altered (not shown). This is consistent with the notion that an additional protein(s) indigenous to myocytes but not present in HEK293 cells (*e.g.* β-subunit) is required for the appearance of late I_{Na} (26–30).

These data also suggest that the phosphorylation status of Ser-516 and Thr-594 on $Na_V1.5$, even in the absence of the β-subunit, is an important mediator of the CaMKII-dependent negative shift in $Na_V1.5$ I_{Na} availability and accumulation of intermediate inactivation.

DISCUSSION

The α-subunit of the human cardiac voltage-gated sodium channel is phosphorylated by CaMKII in the L1 loop. These data are consistent with the L1 region as a hot spot for CaMKII phosphorylation as noted before (14, 15). We show for the first time that activated CaMKII forms a stable interaction with the L1 loop, a targeting mechanism that may contribute to co-localization of CaMKII with $Na_V1.5$ previously observed in myocytes by immunohistochemistry and heart tissue by immunoprecipitation (8, 31). Recently, Ser-571 was identified as an important CaMKII phosphorylation site in L1 (15), a site implicated in regulating $Na_V1.5$ I_{Na}. However, using multiple biochemical assays, we did not observe Ser-571 to be a CaMKII phosphorylation target in our study. Rather, our unbiased measurement of CaMKII phosphorylation sites in L1 identified

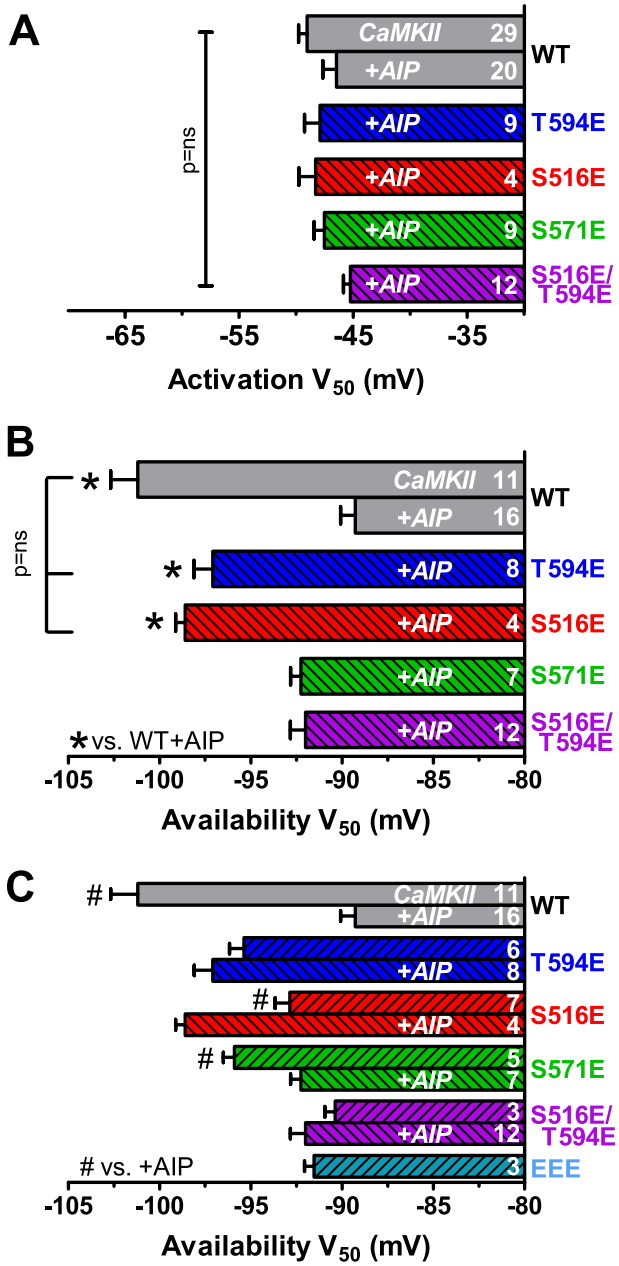

FIGURE 7. **S516E and T594E phosphomimetics shift I_{Na} availability independent of CaMKII.** *A*, V_{50} of activation was not different among phosphomimetics or compared with WT. *B*, T594E and S516E I_{Na} V_{50} of availability was shifted to negative V_m in the presence of AIP and without δ_C-CaMKII co-expression (indicated by *striping*). V_{50} of availability for S571E and S516E/T594E was not significantly different from WT with AIP (*, $p < 0.05$ by ANOVA *versus* WT with AIP; *bracket* indicates no difference by *t* test for S516E and T594E *versus* WT with δ_C-CaMKII). *C*, expanded version of *B*, for comparing the effect of AIP omission (*versus* with AIP) in the pipette for different $Na_V1.5$. For the T594E phosphomimetic, availability was not altered when endogenous CaMKII was allowed to function (*versus* with AIP). For S516E, endogenous CaMKII partly reversed the effect of the phosphomimetic. S571E, which did not mimic the CaMKII-induced shift in V_{50} when AIP was present (in contrast to S516E and T594E) could still shift V_{50} negative by endogenous CaMKII activity. (n as indicated, ±S.E. (*error bars*); AIP and exogenous CaMKII present only where indicated). #, $p < 0.05$ by *t* test *versus* with AIP for the same $Na_V1.5$ type.

three phosphorylation motifs for CaMKII at positions Ser-483/Ser-484, Ser-516, and Thr-594. Unlike Ser-483/Ser-484, the Ser-516 and Thr-594 sites were verified as CaMKII substrates using multiple approaches, including GST fusion mutations of L1 directly, as well as using soluble and immobilized peptides. Thus, these phosphorylation sites were the best candidates for further characterization using functional studies.

To understand the influence of CaMKII phosphorylation of these sites, we co-transfected GFP-δ_C-CaMKII, the predominant cytosolic CaMKII isoform found in the heart, along with WT and mutant forms of $hNa_V1.5$, into HEK293 cells and measured I_{Na} using intracellular pipette conditions supporting acute CaMKII activation (1 μM free Ca^{2+} plus CaM). Interestingly, high Ca^{2+} in the pipette without CaMKII overexpression was sufficient to produce a small but significant hyperpolarizing shift in WT $Na_V1.5$ availability (supplemental Fig. S3). Thus, endogenous CaMKII may be activated by 1 μM pipette Ca^{2+} (32), but higher levels of CaMKII were necessary for maximal functional effects. The potent peptide CaMKII inhibitor AIP was included to verify that changes in I_{Na} were due to CaMKII and not direct effects of Ca^{2+} (33–36) and/or Ca^{2+}/CaM (34, 35, 37–41). We found that Ala point mutations at Ser-516 and Thr-594 identified in our biochemical phosphorylation assays disrupted CaMKII-induced alterations in I_{Na} gating. In further support of Ser-516 and Thr-594 being functionally relevant CaMKII targets, we observed that phosphomimetic mutations (S516E and T594E) functioned to recapitulate CaMKII effects on Na^+ channel availability (in the absence of CaMKII overexpression and presence of AIP).

It is unclear why the Ala mutagenesis data are consistent with both Ser-516 and Thr-594 phosphorylation and Ser-571 presence being required to shift I_{Na} availability, whereas Glu substitution suggests that either Ser-516 or Thr-594 phosphorylation may suffice. Of course, Glu substitution is an imperfect phosphomimetic and the Ser/Thr to Ala mutation might be less supportive of functional competency of phosphorylation at other sites.

Using a biased approach to screen CaMKII phosphorylation sites on $Na_V1.5$ based on the Arg-*X*-*X*-Ser/Thr motif, Hund *et al.* (15) reported that of the mutations tested (including Ser-484, Ser-571, and Ser-664), only S571A blocked CaMKII-dependent regulation of $Na_V1.5$ I_{Na} gating, whereas S571E was reported to mimic WT $Na_V1.5$. We also observed that S571A disrupted CaMKII regulation of I_{Na} gating when CaMKII was co-expressed with the mutant channel. However, unlike S516E and T594E, the S571E mutant was not sufficient to recapitulate CaMKII functional changes in I_{Na} gating when CaMKII was inhibited by AIP. Moreover, S571E channel availability could only shift negative with active CaMKII, suggesting that phosphorylation at other CaMKII target sites (Ser-516 and/or Thr-594) might be required. Thus, although Ser-571 may be a site of phosphorylation, although not by CaMKII in our hands, we suspect that its role in CaMKII-dependent $Na_V1.5$ gating might be less direct than that of Ser-516 and Thr-594. For example, Ser-571 might have an absolute requirement for β_{IV} spectrin to allow CaMKII to gain access (15), or its direct phosphorylation might be mediated by another kinase. Notably, this site is conserved among animal species and other $Na_V1.X$ isoforms (supplemental Fig. S4). Moreover, bioinformatic screening indicates that Ser-571 could be a target for PKA, Akt, or PKG. Further work is required to clarify Ser-571 phosphorylation.

Whether the CaMKII regulatory sites identified in our study are simultaneously, sequentially, or individually phosphorylated *in vivo* by CaMKII is unclear at this point. The simplest interpretation of Fig. 5*E* would be that Ser-516, Ser-571, and Thr-594 must all be phosphorylated to produce the I_{Na} availability effects observed here. These data made it surprising that either T594E or S516E alone could recapitulate CaMKII-dependent I_{Na} availability shifts, whereas these sites appear additive in their effects on accumulation into intermediate inactivation. The ability of the S516E/T594E double phosphomimetic to fully recapitulate CaMKII effects of enhanced accumulation into intermediate inactivation in Fig. 6 but not the shift in I_{Na} availability (Fig. 7*B*) reinforces the complexity and dynamic nature of phosphorylative regulation at these sites. Additional work and new tools, including the use of myocytes, could further clarify this (*e.g.* kinetics and sequence of site phosphorylation, channel state dependence effects). An intriguing possibility is that, as seen for neuronal $K_V1.2$ channel gating (42), graded regulation of $Na_V1.5$ by phosphorylation may also regulate myocyte excitability via modulation of $Na_V1.5$ gating. It is currently unclear whether the presence of multiple phosphorylatable sites in the L1 region of $Na_V1.5$ represents redundancy or permits fine tuning and/or cross-talk between multiple protein kinases.

Notably, Thr-594 in L1 is perfectly conserved among the seven mammalian $Na_V1.5$ channels (supplemental Fig. S4*A*). Among other $Na_V1.X$ channels (supplemental Fig. S4*B*), only SCN8A ($Na_V1.6$) has the Thr-594 equivalent and also the basic Arg/Lys at the P−3 position (most others have Met at P−3 or Ala at the P0). Although Ser-516 is well conserved in $Na_V1.5$ across species, all non-human mammalian $Na_V1.5$ proteins possess a His rather than Arg at P−3, which could alter the ability of CaMKII to phosphorylate this site. Although ClustalW alignment of $Na_V1.X$ channels does not indicate conservation of Ser-516 in the other isoforms, neuronal voltage-gated sodium channels do contain Arg/Lys-*X*-*X*-Ser/Thr motifs in the region upstream from Ser-516 in $Na_V1.5$. Thus, further exploration will be required to determine whether CaMKII also targets the sites studied here in other voltage-gated sodium channels.

We tested for, but did not detect, CaMKII-induced late I_{Na} (not shown). This indicates that $Na_V1.5$ and δ_C-CaMKII alone are not sufficient to recapitulate CaMKII-induced late I_{Na} seen in cardiomyocytes (8, 9, 14). It is possible that CaMKII-induced late I_{Na} involves phosphorylation by CaMKII at the same sites on the sodium channel as studied here but that an additional protein (*e.g.* β-subunit) is required for translation into late I_{Na} (26–30). We also assayed for CaMKII-induced changes in recovery from inactivation but did not observe a significant difference across tested conditions (data not shown). Again, this may reflect the importance of regulatory β-subunits in modulating recovery from inactivation and other gating phenomenon (30, 43–46). Although the use of the heterologous expression system limits the number of functional effects observed, all of the CaMKII-induced functional changes in I_{Na} seen in HEK293 cells are consistent with those observed in myocytes under similar recording conditions (8, 15), indicating that this reduced system can be used to dissect components of CaMKII-dependent functional changes in $Na_V1.5$, and suffice for the CaMKII-induced shifts in availability and intermediate inactivation.

The mechanism underlying the complex functional effects of CaMKII on cardiac sodium channel is of extreme interest because of the therapeutic potential of these targets in arrhythmias and heart failure (47–50). Indeed, the CaMKII-dependent effects on I_{Na} gating in cardiac myocytes (negative-shifted availability curve, accumulated intermediate inactivation, slowed recovery from inactivation, and enhanced late I_{Na}) directly phenocopy a human $Na_V1.5$ arrhythmogenic mutant (Ins1795D), where individual patients exhibit both Brugada syndrome (due to loss of Na^+ channel function at high heart rates and reduced cardiac conduction velocity) and long QT syndrome (where late I_{Na} causes action potential duration prolongation), and both can lead to life-threatening arrhythmias. Because CaMKII expression and activation is elevated in heart failure patients (and animal models of heart failure) (4–7), these CaMKII-dependent alterations in Na^+ channel gating may cause arrhythmogenesis in many millions of people carrying the clinical diagnosis of heart failure. The altered sodium channel gating may also contribute to alterations in intracellular $[Na^+]_i$ and $[Ca^{2+}]_i$ regulation in this same large population, and this can contribute to both systolic and diastolic dysfunction in heart failure. Understanding the molecular and structural details of I_{Na} regulation by CaMKII-dependent phosphorylation will require further work, but our identification of Ser-516 and Thr-594 as functionally important CaMKII target sites on $Na_V1.5$ is a major step forward.

Acknowledgment—We thank Dr. Laurie Parker for assistance with peptide synthesis.

REFERENCES

1. Ruan, Y., Liu, N., and Priori, S. G. (2009) Sodium channel mutations and arrhythmias. *Nat. Rev. Cardiol.* **6,** 337–348
2. Veldkamp, M. W., Viswanathan, P. C., Bezzina, C., Baartscheer, A., Wilde, A. A., and Balser, J. R. (2000) Two distinct congenital arrhythmias evoked by a multidysfunctional Na^+ channel. *Circ. Res.* **86,** E91–E97
3. Abriel, H. (2007) Roles and regulation of the cardiac sodium channel $Na_V1.5$. Recent insights from experimental studies. *Cardiovasc. Res.* **76,** 381–389
4. Hoch, B., Meyer, R., Hetzer, R., Krause, E. G., and Karczewski, P. (1999) Identification and expression of δ-isoforms of the multifunctional Ca^{2+}/calmodulin-dependent protein kinase in failing and nonfailing human myocardium. *Circ. Res.* **84,** 713–721
5. Kirchhefer, U., Schmitz, W., Scholz, H., and Neumann, J. (1999) Activity of cAMP-dependent protein kinase and Ca^{2+}/calmodulin-dependent protein kinase in failing and nonfailing human hearts. *Cardiovasc. Res.* **42,** 254–261
6. Zhang, T., Maier, L. S., Dalton, N. D., Miyamoto, S., Ross, J., Jr., Bers, D. M., and Brown, J. H. (2003) The δC isoform of CaMKII is activated in cardiac hypertrophy and induces dilated cardiomyopathy and heart failure. *Circ. Res.* **92,** 912–919
7. Ai, X., Curran, J. W., Shannon, T. R., Bers, D. M., and Pogwizd, S. M. (2005) Ca^{2+}/calmodulin-dependent protein kinase modulates cardiac ryanodine receptor phosphorylation and sarcoplasmic reticulum Ca^{2+} leak in heart failure. *Circ. Res.* **97,** 1314–1322
8. Wagner, S., Dybkova, N., Rasenack, E. C., Jacobshagen, C., Fabritz, L., Kirchhof, P., Maier, S. K., Zhang, T., Hasenfuss, G., Brown, J. H., Bers, D. M., and Maier, L. S. (2006) Ca^{2+}/calmodulin-dependent protein kinase

II regulates cardiac Na^+ channels. *J. Clin. Invest.* **116,** 3127–3138
9. Maltsev, V. A., Reznikov, V., Undrovinas, N. A., Sabbah, H. N., and Undrovinas, A. (2008) Modulation of late sodium current by Ca^{2+}, calmodulin, and CaMKII in normal and failing dog cardiomyocytes. Similarities and differences. *Am. J. Physiol. Heart Circ. Physiol.* **294,** H1597–H1608
10. Bradshaw, J. M., Hudmon, A., and Schulman, H. (2002) Chemical quenched flow kinetic studies indicate an intraholoenzyme autophosphorylation mechanism for Ca^{2+}/calmodulin-dependent protein kinase II. *J. Biol. Chem.* **277,** 20991–20998
11. Ashpole, N. M., and Hudmon, A. (2011) Excitotoxic neuroprotection and vulnerability with CaMKII inhibition. *Mol. Cell Neurosci.* **46,** 720–730
12. Hudmon, A., Schulman, H., Kim, J., Maltez, J. M., Tsien, R. W., and Pitt, G. S. (2005) CaMKII tethers to L-type Ca^{2+} channels, establishing a local and dedicated integrator of Ca^{2+} signals for facilitation. *J. Cell Biol.* **171,** 537–547
13. Hudmon, A., Choi, J. S., Tyrrell, L., Black, J. A., Rush, A. M., Waxman, S. G., and Dib-Hajj, S. D. (2008) Phosphorylation of sodium channel $Na_V1.8$ by p38 mitogen-activated protein kinase increases current density in dorsal root ganglion neurons. *J. Neurosci.* **28,** 3190–3201
14. Aiba, T., Hesketh, G. G., Liu, T., Carlisle, R., Villa-Abrille, M. C., O'Rourke, B., Akar, F. G., and Tomaselli, G. F. (2010) Na^+ channel regulation by Ca^{2+}/calmodulin and Ca^{2+}/calmodulin-dependent protein kinase II in guinea pig ventricular myocytes. *Cardiovasc. Res.* **85,** 454–463
15. Hund, T. J., Koval, O. M., Li, J., Wright, P. J., Qian, L., Snyder, J. S., Gudmundsson, H., Kline, C. F., Davidson, N. P., Cardona, N., Rasband, M. N., Anderson, M. E., and Mohler, P. J. (2010) A β(IV)-spectrin/CaMKII signaling complex is essential for membrane excitability in mice. *J. Clin. Invest.* **120,** 3508–3519
16. Pawson, T., and Scott, J. D. (1997) Signaling through scaffold, anchoring, and adaptor proteins. *Science* **278,** 2075–2080
17. Strack, S., and Colbran, R. J. (1998) Autophosphorylation-dependent targeting of calcium/calmodulin-dependent protein kinase II by the NR2B subunit of the *N*-methyl-D-aspartate receptor. *J. Biol. Chem.* **273,** 20689–20692
18. Bayer, K. U., De Koninck, P., Leonard, A. S., Hell, J. W., and Schulman, H. (2001) Interaction with the NMDA receptor locks CaMKII in an active conformation. *Nature* **411,** 801–805
19. Grueter, C. E., Abiria, S. A., Wu, Y., Anderson, M. E., and Colbran, R. J. (2008) Differential regulated interactions of calcium/calmodulin-dependent protein kinase II with isoforms of voltage-gated calcium channel β subunits. *Biochemistry* **47,** 1760–1767
20. Songyang, Z., Lu, K. P., Kwon, Y. T., Tsai, L. H., Filhol, O., Cochet, C., Brickey, D. A., Soderling, T. R., Bartleson, C., Graves, D. J., DeMaggio, A. J., Hoekstra, M. F., Blenis, J., Hunter, T., and Cantley, L. C. (1996) A structural basis for substrate specificities of protein Ser/Thr kinases. Primary sequence preference of casein kinases I and II, NIMA, phosphorylase kinase, calmodulin-dependent kinase II, CDK5, and Erk1. *Mol. Cell Biol.* **16,** 6486–6493
21. White, R. R., Kwon, Y. G., Taing, M., Lawrence, D. S., and Edelman, A. M. (1998) Definition of optimal substrate recognition motifs of Ca^{2+}-calmodulin-dependent protein kinases IV and II reveals shard and distinctive features. *J. Biol. Chem.* **273,** 3166–3172
22. Frank, R., and Overwin, H. (1996) SPOT synthesis. Epitope analysis with arrays of synthetic peptides prepared on cellulose membranes. *Methods Mol. Biol.* **66,** 149–169
23. Frank, R. (2002) The SPOT synthesis technique. Synthetic peptide arrays on membrane supports. Principles and applications. *J. Immunol. Methods* **267,** 13–26
24. Naffin, J. L., Han, Y., Olivos, H. J., Reddy, M. M., Sun, T., and Kodadek, T. (2003) Immobilized peptides as high-affinity capture agents for self-associating proteins. *Chem. Biol.* **10,** 251–259
25. Obenauer, J. C., Cantley, L. C., and Yaffe, M. B. (2003) Scansite 2.0: Proteome-wide prediction of cell signaling interactions using short sequence motifs. *Nucleic Acids Res.* **31,** 3635–3641
26. Aman, T. K., Grieco-Calub, T. M., Chen, C., Rusconi, R., Slat, E. A., Isom, L. L., and Raman, I. M. (2009) Regulation of persistent Na current by interactions between β subunits of voltage-gated Na channels. *J. Neurosci.* **29,** 2027–2042
27. Qu, Y., Curtis, R., Lawson, D., Gilbride, K., Ge, P., DiStefano, P. S., Silos-Santiago, I., Catterall, W. A., and Scheuer, T. (2001) Differential modulation of sodium channel gating and persistent sodium currents by the β1, β2, and β3 subunits. *Mol. Cell Neurosci.* **18,** 570–580
28. Bant, J. S., and Raman, I. M. (2010) Control of transient, resurgent, and persistent current by open-channel block by Na channel β4 in cultured cerebellar granule neurons. *Proc. Natl. Acad. Sci. U.S.A.* **107,** 12357–12362
29. Maltsev, V. A., Kyle, J. W., and Undrovinas, A. (2009) Late Na^+ current produced by human cardiac Na^+ channel isoform $Na_V1.5$ is modulated by its β1 subunit. *J. Physiol. Sci.* **59,** 217–225
30. Mishra, S., Undrovinas, N. A., Maltsev, V. A., Reznikov, V., Sabbah, H. N., and Undrovinas, A. (2011) Post-transcriptional silencing of *SCN1B* and *SCN2B* genes modulates late sodium current in cardiac myocytes from normal dogs and dogs with chronic heart failure. *Am. J. Physiol. Heart Circ. Physiol.* **301,** H1596–H1605
31. Yoon, J. Y., Ho, W. K., Kim, S. T., and Cho, H. (2009) Constitutive CaMKII activity regulates Na+ channel in rat ventricular myocytes. *J. Mol. Cell Cardiol.* **47,** 475–484
32. Tsui, J., Inagaki, M., and Schulman, H. (2005) Calcium/calmodulin-dependent protein kinase II (CaMKII) localization acts in concert with substrate targeting to create spatial restriction for phosphorylation. *J. Biol. Chem.* **280,** 9210–9216
33. Wingo, T. L., Shah, V. N., Anderson, M. E., Lybrand, T. P., Chazin, W. J., and Balser, J. R. (2004) An EF-hand in the sodium channel couples intracellular calcium to cardiac excitability. *Nat. Struct. Mol. Biol.* **11,** 219–225
34. Shah, V. N., Wingo, T. L., Weiss, K. L., Williams, C. K., Balser, J. R., and Chazin, W. J. (2006) Calcium-dependent regulation of the voltage-gated sodium channel hH1. Intrinsic and extrinsic sensors use a common molecular switch. *Proc. Natl. Acad. Sci. U.S.A.* **103,** 3592–3597
35. Young, K. A., and Caldwell, J. H. (2005) Modulation of skeletal and cardiac voltage-gated sodium channels by calmodulin. *J. Physiol.* **565,** 349–370
36. Chagot, B., Potet, F., Balser, J. R., and Chazin, W. J. (2009) Solution NMR structure of the C-terminal EF-hand domain of human cardiac sodium channel $Na_V1.5$. *J. Biol. Chem.* **284,** 6436–6445
37. Mori, M., Konno, T., Morii, T., Nagayama, K., and Imoto, K. (2003) Regulatory interaction of sodium channel IQ-motif with calmodulin C-terminal lobe. *Biochem. Biophys. Res. Commun.* **307,** 290–296
38. Theoharis, N. T., Sorensen, B. R., Theisen-Toupal, J., and Shea, M. A. (2008) The neuronal voltage-dependent sodium channel type II IQ motif lowers the calcium affinity of the C-domain of calmodulin. *Biochemistry* **47,** 112–123
39. Kim, J., Ghosh, S., Liu, H., Tateyama, M., Kass, R. S., and Pitt, G. S. (2004) Calmodulin mediates Ca^{2+} sensitivity of sodium channels. *J. Biol. Chem.* **279,** 45004–45012
40. Tan, H. L., Kupershmidt, S., Zhang, R., Stepanovic, S., Roden, D. M., Wilde, A. A., Anderson, M. E., and Balser, J. R. (2002) A calcium sensor in the sodium channel modulates cardiac excitability. *Nature* **415,** 442–447
41. Deschênes, I., Neyroud, N., DiSilvestre, D., Marbán, E., Yue, D. T., and Tomaselli, G. F. (2002) Isoform-specific modulation of voltage-gated Na^+ channels by calmodulin. *Circ. Res.* **90,** E49–E57
42. Park, K. S., Mohapatra, D. P., Misonou, H., and Trimmer, J. S. (2006) Graded regulation of the Kv2.1 potassium channel by variable phosphorylation. *Science* **313,** 976–979
43. Ko, S. H., Lenkowski, P. W., Lee, H. C., Mounsey, J. P., and Patel, M. K. (2005) Modulation of Na(v) 1.5 by β1- and β3-subunit co-expression in mammalian cells. *Pflugers Arch.* **449,** 403–412
44. Fahmi, A. I., Patel, M., Stevens, E. B., Fowden, A. L., John, J. E., 3rd, Lee, K., Pinnock, R., Morgan, K., Jackson, A. P., and Vandenberg, J. I. (2001) The sodium channel β-subunit SCN3b modulates the kinetics of SCN5a and is expressed heterogeneously in sheep heart. *J. Physiol.* **537,** 693–700
45. Meadows, L. S., Chen, Y. H., Powell, A. J., Clare, J. J., and Ragsdale, D. S. (2002) Functional modulation of human brain $Na_V1.3$ sodium channels, expressed in mammalian cells, by auxiliary β1, β2, and β3 subunits. *Neuroscience* **114,** 745–753

46. Goldin, A. L. (2003) Mechanisms of sodium channel inactivation. *Curr. Opin. Neurobiol.* **13,** 284–290
47. Bers, D. M., and Grandi, E. (2009) Calcium/calmodulin-dependent kinase II regulation of cardiac ion channels. *J. Cardiovasc. Pharmacol.* **54,** 180–187
48. Anderson, M. E., Brown, J. H., and Bers, D. M. (2011) CaMKII in myocardial hypertrophy and heart failure. *J. Mol. Cell Cardiol.* **51,** 468–473
49. Grueter, C. E., Colbran, R. J., and Anderson, M. E. (2007) CaMKII, an emerging molecular driver for calcium homeostasis, arrhythmias, and cardiac dysfunction. *J. Mol. Med.* **85,** 5–14
50. Maier, L. S. (2011) CaMKII regulation of voltage-gated sodium channels and cell excitability. *Heart Rhythm* **8,** 474–477